



Full Current-Type Control-Based Hybrid Energy Storage System

Jiahui Ren ¹, Wenli Lin ², Xinbo Liu ¹, Shuiyuan He ¹, Zhonghao Dongye ¹ and Lijun Diao ^{1,*}

¹ School of Electrical Engineering, Beijing Jiaotong University, Beijing 100044, China; 19121485@bjtu.edu.cn (J.R.); 20121466@bjtu.edu.cn (X.L.); 21126128@bjtu.edu.cn (S.H.); dyzh@bjtu.edu.cn (Z.D.)

² Beijing Institute of Spacecraft System Engineering, Beijing 100094, China; tarrsh@163.com

* Correspondence: ljdiao@bjtu.edu.cn

Abstract: With greater power density, a hybrid power source that combines supercapacitors and batteries has a wide range of applications in pulse-operated power systems. In this paper, a supercapacitor/battery semi-active hybrid energy storage system (HESS) with a full current-type control strategy is presented. The studied HESS is composed of batteries, supercapacitors, and a bidirectional buck–boost converter. The converter is controlled such that supercapacitors supply load power pulses, and batteries provide the power in steady state. To realize the fast compensation of the supercapacitors to the load power pulses, a power distribution module based on hysteresis control theory is designed in the control system. Moreover, the control strategy does not require the model parameters of the converter and supercapacitors, so the control system is simplified. A complete configuration scheme and cost analysis of the proposed HESS are also presented. Obtained results show that the proposed supercapacitor/battery semi-active HESS has good performance in terms of dynamic response, weight, and energy utilization coefficient (EUC).

Keywords: hybrid energy storage system; pulsed load; bidirectional buck–boost converter; Li-ion battery; supercapacitor



Citation: Ren, J.; Lin, W.; Liu, X.; He, S.; Dongye, Z.; Diao, L. Full Current-Type Control-Based Hybrid Energy Storage System. *Energies* **2022**, *15*, 2910. <https://doi.org/10.3390/en15082910>

Academic Editor: Nicu Bizon

Received: 24 March 2022

Accepted: 13 April 2022

Published: 15 April 2022

Publisher's Note: MDPI stays neutral with regard to jurisdictional claims in published maps and institutional affiliations.



Copyright: © 2022 by the authors. Licensee MDPI, Basel, Switzerland. This article is an open access article distributed under the terms and conditions of the Creative Commons Attribution (CC BY) license (<https://creativecommons.org/licenses/by/4.0/>).

1. Introduction

The battery energy storage system (BESS) with a Li-ion battery as the core device has become the mainstream power supply scheme, due to its high energy density and decreasing cost [1]. However, limited by the low power density of Li-ion batteries, BESS used for pulsed power loads such as electric vehicles and satellites faces the problems of excessive battery size and weight [2,3]. Since supercapacitors have high specific power and can be charged and discharged quickly, which are very suitable for the pulsed loads, the HESS combining Li-ion batteries and supercapacitors has been widely studied [4].

In HESS, supercapacitors provide load current pulses instead of batteries, so the battery pack can be miniaturized. Proper energy management strategy (EMS) and component configuration can reduce the weight and lifecycle cost of the energy storage system while improving the payload capabilities and capacity utilization [1,5].

The topology, control strategy, and optimal configuration of HESS have always been important research content. In recent years, several topologies have been proposed, which can be divided into passive topology, semi-active topology, and fully active topology according to the combination mode of battery and supercapacitor [5–7]. The battery is directly paralleled with the supercapacitor as the DC power source in passive HESS, without any power converters. This topology is very simple, but due to the lack of control, the power compensation effect of the supercapacitor is relatively poor [6,8]. In contrast, fully active HESS has the best performance, as it employs two DC–DC converters for energy management of the battery and the supercapacitor, respectively. Nonetheless, this topology has high costs, and the real-time interaction control between the two converters is complex [9–11]. The semi-active HESS only employs one power converter, and although

its control performance is not perfect, the cost and complexity of the system are greatly reduced. Furthermore, most control strategies can be applied to this topology. Due to these advantages, semi-active HESS is currently the most popular topology [12,13]. There are two semi-active HESS topologies. One topology is to connect a DC–DC converter between the supercapacitor and the DC bus, connecting the Li-ion battery directly to the DC bus. This configuration efficiently utilizes the energy of the supercapacitor, but the DC bus voltage cannot be changed. Another topology is to connect a DC–DC converter between the Li-ion battery and the DC bus, connecting the supercapacitor directly to the DC bus. This structure protects the battery but limits the operating range of the supercapacitor [5].

A variety of control strategies have been designed and studied, and the basic principles of these strategies are similar due to the simple structure of HESS. In [14], a current-type polynomial dynamic control strategy for supercapacitor/battery semi-active HESS was proposed, and the output power of the DC–DC converter was regulated by controlling the supercapacitor current. This strategy calculates the supercapacitor current reference using the DC–DC converter model, and the converter efficiency parameters in the model are corrected online. Since the efficiency parameters of the converter are simultaneously affected by many factors such as duty cycle, input power, voltage, and current, the output power of the DC–DC converter may not be precisely controlled using the supercapacitor current as a reference. In [15], a control algorithm based on power filter theory was presented, and the high- and low-frequency components of the load power were allocated to the supercapacitor and battery, respectively. Since the equivalent series resistance (ESR) of the supercapacitor pack is introduced into the control loop, the accuracy of this control algorithm may be affected when the supercapacitor cells increase. In [16], a control strategy based on the current filter algorithm was designed, which limited the battery current by adjusting the cut-off frequency. In addition, some online high-performance control algorithms have also been applied to HESS, such as model predictive control and fuzzy logic control [17–19].

The optimal configuration of HESS mainly considers cost, battery lifetime, and the total weight of the energy storage devices. In [11,12], the operation cost of HESS was considered as the optimization object, which could be reduced by 50%, compared with that of BESS. The authors of [3] proposed a hybrid optimization algorithm to calculate the feasible optimal solution under the joint constraints of weight, cost, and battery lifetime. In [1], an optimization algorithm based on the Hamiltonian function was designed to solve the optimal pack size of the HESS configuration. In addition, the dynamic programming algorithm and Pontryagin's minimum principle were also used to reduce the operation cost and size of HESS [20].

Since most of the energy management strategies of HESS rely on the model of power converters, it is necessary to modify the model parameters online for ensuring the control accuracy, which increases the computational cost. In this paper, an improved full current-type polynomial control strategy is proposed for semi-active HESS. This method takes the bidirectional DC–DC converter as the controlled object and directly controls the converter current, which simplifies the control system, and the control accuracy is independent of the model parameters.

This paper is organized as follows: First, combining the HESS model with the optimization objective of the total weight of the energy storage devices, a conventional configuration scheme is established. Then, a full current-type DC–DC converter control strategy is proposed for energy management. Finally, simulation and experiment are used to evaluate the proposed control strategy and configuration scheme.

2. HESS Configuration Model

Figure 1 shows the basic topology of supercapacitor/battery semi-active HESS. In this paper, a non-isolated, bidirectional buck–boost converter was employed. The Li-ion battery is directly connected to the DC bus to provide energy and stabilize the DC bus voltage, while the supercapacitor is interfaced to the DC bus with a bidirectional DC–DC

converter to compensate for the peak load power. The converter operates in buck mode when the supercapacitor is charged while operating in boost mode when the supercapacitor discharges.

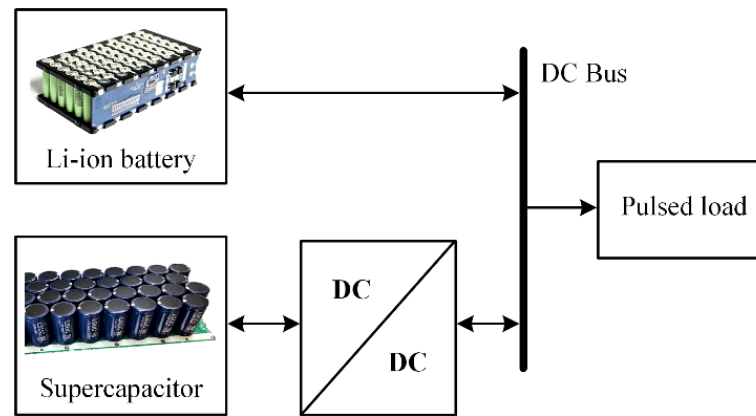


Figure 1. Supercapacitor/battery semi-active HESS topology.

2.1. Battery Pack Design Considerations

The power allocation rules should be established first. A typical approach is to obtain the high-frequency component of the load power through a signal filter and then control the supercapacitor to output this high-frequency power and the battery pack to output the remaining low-frequency power [11,15]. However, the battery current of this method is indeterminate and depends on the filter cut-off frequency and the actual load power. Therefore, the distribution method based on the current level was adopted. In the process of HESS providing a power pulse, the battery current is fixed, and the supercapacitor outputs most of the pulse current via the converter.

The battery pack was designed according to the DC bus voltage, the total energy consumption during the load operation, and the maximum power allocated.

The voltage of the DC bus is fixed by the battery pack, and the battery pack voltage is obtained using the following equation, where $V_{pack,Li}$ is the battery pack voltage, and V_{dcbus} is the DC bus voltage:

$$V_{pack,Li} = V_{dcbus}, \quad (1)$$

The battery pack should provide the energy consumed by the pulsed power during a mission. In order to ensure the performance and lifetime, the depth of discharge (DOD) of the Li-ion battery pack cannot exceed 80% [21]. The rated energy of the battery pack can be denoted as in (2), where $E_{pack,Li}$ is the energy of the battery pack; $P_{L,norm}$ and $P_{L,peak}$ are the normal power and peak power of the pulsed load, respectively. η_{conv} is the power converter efficiency, I is the duration of load operation, $DOD_{pack,Li}$ is the DOD of battery pack, and k_{Li} is the margin coefficient of battery pack.

$$E_{pack,Li} = k_{Li} \frac{\int_0^I \left(P_{L,norm}(t) + \frac{P_{L,peak}(t)}{\eta_{conv}^2} \right) dt}{DOD_{pack,Li}}, \quad (2)$$

The battery power is composed of the normal load power and the charging power of the supercapacitor, which can be expressed as follows, where $P_{SC,charge}$ is the supercapacitor charging power:

$$P_{pack,Li} = k_{Li} \left(P_{L,norm} + \frac{P_{SC,charge}}{\eta_{conv}} \right), \quad (3)$$

2.2. Supercapacitor Pack Design Considerations

Since the supercapacitor has a strong instantaneous power capability, its design mainly considers the maximum load energy pulse and voltage constraints [22,23]. Additionally, the rated energy of the supercapacitor pack can be described as

$$E_{pack,SC} = k_{SC} \frac{\int_0^{t_{peak}} \frac{P_{L,peak}(t)}{\eta_{conv}} dt}{DOD_{pack,SC}}, \quad (4)$$

where $E_{pack,SC}$ is the rated energy of supercapacitor pack; t_{peak} is the duration of single peak power; $DOD_{pack,SC}$ and k_{SC} are the DOD and margin coefficient of supercapacitor pack, respectively. Since the charging and discharging of supercapacitors is a physical process, supercapacitors can theoretically be fully discharged. Generally, the $DOD_{pack,SC}$ can reach more than 90%.

Limited by the power loss and cooling system of the DC–DC converter, the voltage of the supercapacitor pack should not be too low, and a reasonable voltage range is as follows [1], where $V_{min,conv}$ is the minimum voltage of the supercapacitor pack that the DC–DC converter can operate safely, and $V_{pack,SC}$ is the rated supercapacitor pack voltage:

$$V_{min,conv} \leq V_{pack,SC} \leq V_{dcbus}, \quad (5)$$

2.3. Configuration Scheme

Regardless of V_{dcbus} , the configuration of the battery pack and supercapacitor pack are unrelated. Assuming homogeneity of Li-ion cell and supercapacitor cell, combining (1)–(3), the cell numbers and structure of the battery pack should satisfy the constraints in (6), where $N_{s,Li}$ is the number of Li-ion cells in series, $N_{p,Li}$ is the number of Li-ion cells in parallel; $V_{cell,Li}$ and $C_{cell,Li}$ are the rated voltage and capacity of a single Li-ion cell, respectively. Additionally, μ is the discharge rate of the battery.

$$\begin{cases} N_{s,Li} \cdot V_{cell,Li} = V_{dcbus} \\ V_{cell,Li} \cdot C_{cell,Li} \cdot N_{s,Li} \cdot N_{p,Li} \geq E_{pack,Li} \\ \mu \cdot V_{cell,Li} \cdot C_{cell,Li} \cdot N_{s,Li} \cdot N_{p,Li} \geq P_{pack,Li} \end{cases}, \quad (6)$$

In the same way, combining (4) and (5), the constraints on the cell numbers and structure of the supercapacitor pack can be obtained with the equation below, where $N_{s,SC}$ is the number of supercapacitor cells in series, $N_{p,SC}$ is the number of supercapacitor cells in parallel, and $V_{cell,sc}$ and $C_{cell,sc}$ are the rated voltage and capacitance of a single supercapacitor cell, respectively.

$$\begin{cases} \frac{1}{2} C_{cell,SC} \cdot V_{cell,SC}^2 \cdot N_{s,SC} \cdot N_{p,SC} \geq E_{pack,SC} \\ V_{min,conv} \leq N_{s,SC} \cdot V_{cell,SC} \leq V_{dc bus} \end{cases}, \quad (7)$$

According to the constraint conditions in (6) and (7), the optimal configuration can be obtained as

$$\begin{cases} N_{s,Li} = \frac{V_{dcbus}}{V_{cell,Li}} \\ N_{p,Li} = \max \left\{ \frac{P_{pack,Li}}{\mu \cdot V_{dcbus} \cdot C_{cell,Li}}, \frac{E_{pack,Li}}{V_{dcbus} \cdot C_{cell,Li}} \right\} \\ N_{s,SC} \in \left(\frac{V_{min,conv}}{V_{cell,SC}}, \frac{V_{dcbus}}{V_{cell,SC}} \right) \\ N_{p,SC} = \frac{2E_{pack,SC}}{N_{s,SC} \cdot C_{cell,SC} \cdot V_{cell,SC}^2} \end{cases}, \quad (8)$$

Additionally, the minimum weight of the battery pack and the supercapacitor pack can be expressed as (9). Notably, the weights of the battery management system (BMS) and assembly box were not included.

$$\begin{cases} W_{pack,Li} = N_{s,Li} \cdot N_{p,Li} \cdot W_{cell,Li} \\ W_{pack,SC} = N_{s,SC} \cdot N_{p,SC} \cdot W_{cell,SC} \end{cases}, \quad (9)$$

where $W_{pack,Li}$ and $W_{pack,SC}$ are the weights of the Li-ion battery pack and supercapacitor pack, respectively. Additionally, $W_{cell,Li}$ and $W_{cell,SC}$ are the weights of Li-ion cell and supercapacitor cell, respectively.

3. DC–DC Converter and Control

3.1. Converter Topology

In this paper, a bidirectional synchronous rectifier buck–boost converter was adopted to improve efficiency [24], and the topology is shown in Figure 2. During buck mode, Q_1 was used as the main switch and Q_2 served as the assistant free-wheeling switch. While during boost mode, Q_2 was the main switch, and Q_1 served as the assistant switch. In the continuous conduction mode (CCM), the driving signals of Q_1 and Q_2 were complementary.

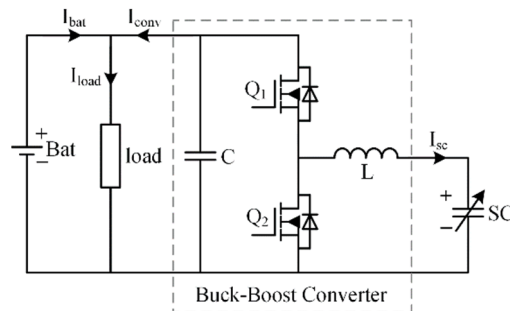


Figure 2. Bidirectional synchronous rectifier buck–boost converter.

It should be noted that both battery and supercapacitor are active loads, during soft starting, the converter will operate in discontinuous conduction mode (DCM) due to the small duty cycle of the main switch. In DCM, if the auxiliary switch is not turned off in time, the inductor current will flow backward; consequently, the converter efficiency is diminished, and the battery and switches will also be damaged as the current backflow increases. Different from the absolutely complementary drive of CCM, in DCM, the auxiliary switch needs to be turned off when the inductor current returns to zero [25].

3.2. Supercapacitor Model

Figure 3 shows a simple equivalent circuit model of the supercapacitor pack, which consists of the capacitor C , the equivalent series resistor R_{es} , and the equivalent parallel resistor R_{ep} [26]. According to this model, the relationship between the supercapacitor pack voltage V_{SC} and the voltage V_C representing the real energy can be obtained with (10), where I_{SC} is the supercapacitor current, and since R_{ep} is very large, its influence on V_{SC} is neglected. It must be noted that when I_{SC} is not zero, the directly measured V_{SC} cannot reflect the actually stored energy of the supercapacitor. Therefore, it is necessary to combine V_{SC} and I_{SC} to calculate accurate ultracapacitor charging status.

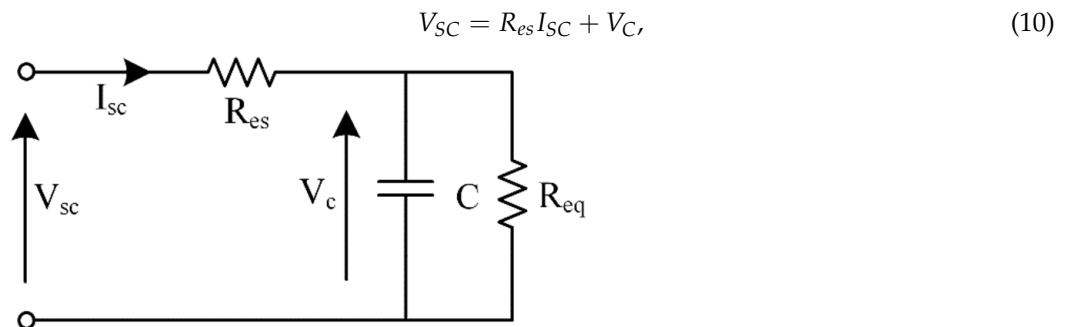


Figure 3. Equivalent circuit model of supercapacitor.

3.3. Control Strategy

The bidirectional buck–boost converter is controlled according to the control strategy described in Figure 4a. In buck operation mode, the supercapacitor pack is charged to ensure that there is enough energy to support the load power pulse later, and I_{SC} is controlled in a closed loop. In boost operation mode, I_{conv} is closed-loop controlled to satisfy the peak current requirement of the load. Since the load current I_{load} is given, the battery current I_{bat} is also controlled using (11).

$$I_{bat} = I_{load} - I_{conv}, \tag{11}$$

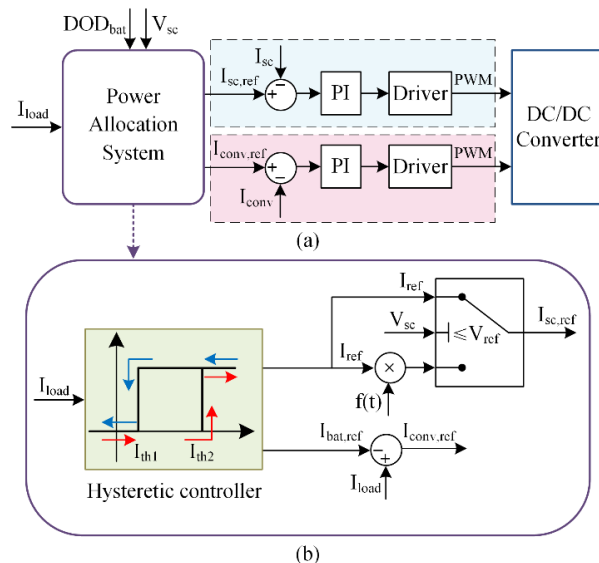


Figure 4. Control and power allocation of HESS: (a) block diagram of the DC–DC converter control; (b) diagram explaining the power allocation system.

The power allocation system shown in Figure 4b determines the operation mode of the DC–DC converter, and the reference currents of the converter and supercapacitors ($I_{conv,ref}$ and $I_{sc,ref}$, respectively) are also given. As the bus voltage is fixed, a controller based on the hysteresis comparison principle is applied to the load current to assess the load power level.

Figure 5 demonstrates a complete flowchart of the proposed power allocation system. Define I_{th1} and I_{th2} as the lower threshold and upper threshold of the hysteresis comparator. If $I_{load} < I_{th1}$, the load runs at normal power, and at this stage, the converter should operate in buck mode to charge the supercapacitors. The charging process can be divided into two phases.

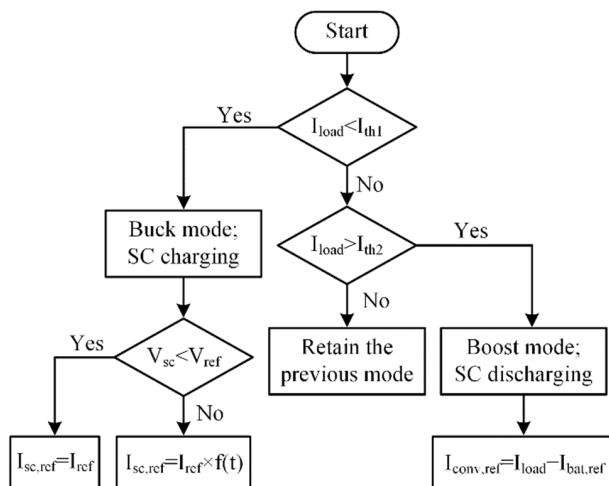


Figure 5. Flowchart of the power allocation system.

In the first phase, the commonly used constant current charging is employed, and the supercapacitors' current reference $I_{SC,ref} = I_{ref}$ is obtained. According to the previous analysis, due to the influence of R_{es} , the charging status calculated by the measured V_{SC} is slightly less than the target charging status. Therefore, a second stage of charging is required after the measured V_{SC} reaches the target voltage V_{ref} . During the second phase, the charging current gradually decreases, and $I_{SC,ref}$ is calculated as

$$I_{SC} = I_{ref} \times f(t), \quad (12)$$

where $f(t)$ is a decreasing linear function, with an initial value of 1 and a final value of 0. The maximum battery current $I_{bat,max}$ can be described as

$$I_{bat,max} = \frac{P_{L,norm} + I_{ref} \cdot V_{ref} / \eta_{conv}}{V_{dcbus}}, \quad (13)$$

If $I_{load} > I_{th2}$, the load operates at peak power, and at this stage, the converter should operate in boost mode and the supercapacitor pack starts discharging. The purpose of this stage is to replace the battery pack with the supercapacitors to provide the peak load current, so the battery current I_{bat} is limited as $I_{bat,ref}$ and the converter current reference $I_{conv,ref}$ is obtained as

$$I_{conv,ref} = I_{load} - I_{bat,ref}, \quad (14)$$

4. Simulation Results

To verify the performance of the control strategy proposed in Section 3, a supercapacitor/battery HESS shown in Figure 1 was established in the MATLAB/SIMULINK.

The peak load power was 2 kW, and the normal load power was 0.12 kW. The load cycle duration was 40 s, $P_{L,peak}$ duration was 5 s, $P_{L,norm}$ duration was 35 s, and the load ran continuously for one hour under the above conditions. The battery pack had a rated voltage of 72 V and a rated capacity of 9.6 Ah, the rated voltage of the supercapacitor pack was 56 V, and the capacitance was 17.5 F. Table 1 shows the values of the main circuit parameters.

Table 1. Parameters used in the simulation and experiment.

Parameters	Symbol	Value
Battery pack		72 V/9.6 Ah
Supercapacitor pack		56 V/17.5 F
Inductor	L	200 μ H
Output capacitor	C	220 μ F
Switching frequency	f_s	50 kHz

Figure 6 shows the simulation result of the supercapacitor's current control in buck mode. In the beginning, the supercapacitor current reference $I_{SC,ref}$ was fixed at 8 A, and then $I_{SC,ref}$ gradually reduced from 8 A to 0 A. This figure shows that the supercapacitor's current-control strategy is satisfactory.

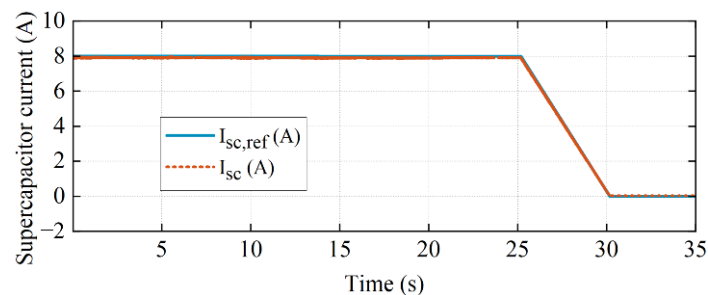


Figure 6. Simulation result of the supercapacitor's current control.

Figure 7 shows the simulation result of the converter's current control in boost mode. In this paper, the peak load power was intended to be provided by the supercapacitor pack alone, so the battery current reference $I_{bat,ref}$ was fixed at 0 A, and the sampled load current I_{load} was taken as the converter current reference $I_{conv,ref}$. Since the battery pack was connected to the load, the control accuracy was bound to be affected. However, it can be seen from Figure 7 that almost all of the peak load current was provided by the converter, meaning that the converter's current-control strategy was satisfactory.

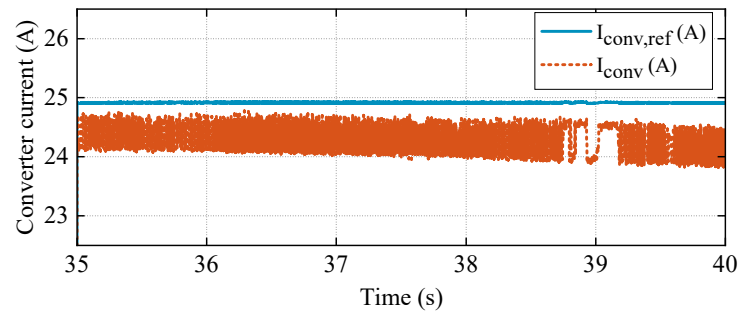


Figure 7. Simulation result of the converter current control.

The simulation results of battery current and load current in a load cycle are shown in Figure 8. The peak load current was 24.92 A, while the maximum output current of the battery pack was only 7.36 A, which was reduced by 17.57 A, compared with the former. These results mean that the peak current stress of the battery pack greatly decreased by using HESS.

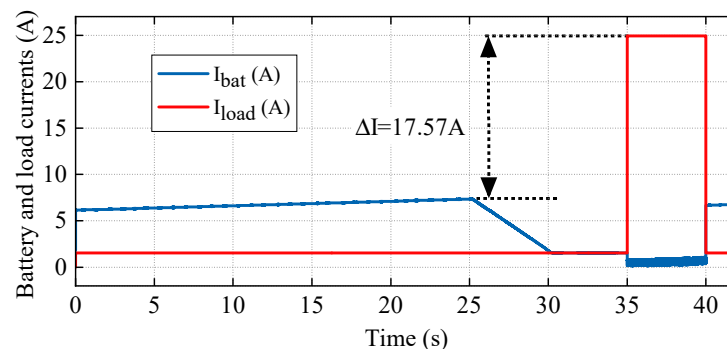


Figure 8. Simulation results of the battery current and load current.

5. Experimental Results

To evaluate the supercapacitor/battery semi-active HESS with a full current-type control strategy, an experimental platform was built, which consists of the pulsed power load, a Li-ion battery pack, a supercapacitor pack, a bidirectional buck–boost converter, and the control system based on STM32F103C8T6 microprocessor. The 2 kw peak power experimental platform is shown in Figure 9. All circuit parameters are consistent with Table 1.

For safety reasons, the supercapacitor pack voltage ranged from 40 V to 56 V in the experiment, so the current through the DC–DC converter was not more than 50 A.

Figure 10 shows the experimental waveforms of battery current and load current in a load cycle. The normal current of the pulse load was 1.55 A, and the peak current was 25.6 A. When the load was running at normal power, the battery provided the power for charging the supercapacitors and normal operation of the load. Considering the current ripple, the maximum battery current $I_{bat,max}$ was 8.5 A. When the load was running at peak power, the battery current was successfully limited to around 0 A, and almost all of the peak load current was provided by the supercapacitors with the boost converter.

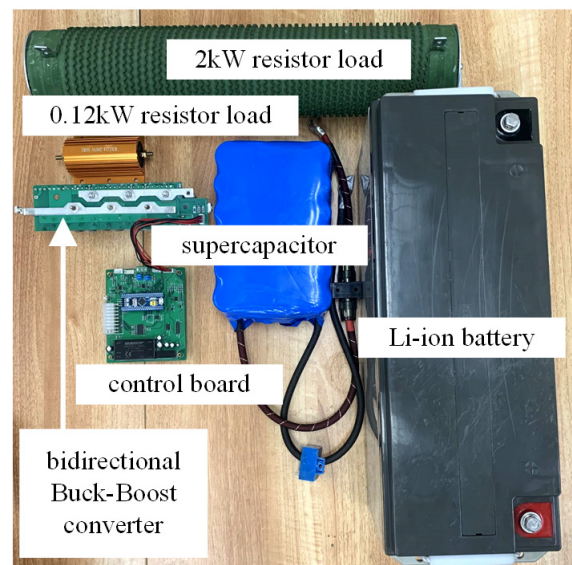


Figure 9. The experimental platform with 2 kw peak power.

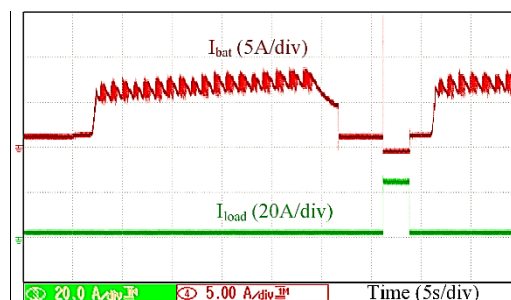


Figure 10. Experimental waveforms of battery current and load current.

The voltage and current experimental waveforms of the supercapacitors in a load cycle are shown in Figure 11. The initial voltage of the supercapacitor pack was 40 V, and it was charged to the target voltage of 54 V at a constant current of 8 A. After that, the charging current gradually decreased, and the charging process was terminated immediately when the voltage reached the upper limit of 56 V. Five seconds after the end of charging, the load current suddenly increased, the DC–DC converter switched from buck mode to boost mode, and the supercapacitors began to discharge. The initial discharge current was 40.5 A, and the maximum discharge current was 48.1 A.

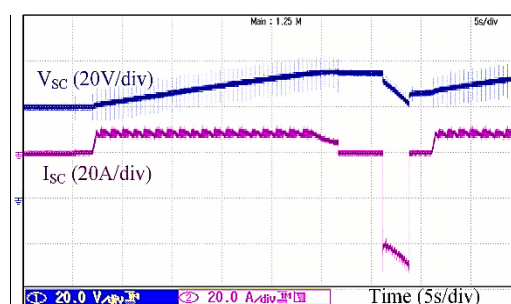


Figure 11. Experimental waveforms of supercapacitors voltage and supercapacitors current.

At the moment when the supercapacitors discharge started and ended, the terminal voltage V_{SC} dropped and rose suddenly, with amplitudes of 3.1 V and 4.0 V, respectively. This phenomenon is mainly caused by the equivalent series resistance R_{es} of the supercapacitors. As described in (10), at the moment of supercapacitors discharge, due to the sudden increase

in the current I_{SC} , the voltage drop on R_{es} increased, so V_{SC} dropped. Similarly, when the discharge ended, the voltage drop on R_{es} was reduced to 0 V, so V_{SC} suddenly increased.

Figure 12a shows the experimental waveforms during the dynamic process through which the DC–DC converter switched from buck mode to boost mode. Within 4 milliseconds after the load current increased, the supercapacitors had completely replaced the battery pack to provide peak load power. Figure 12b shows the experimental results during the dynamic process through which the DC–DC converter switched from boost mode to buck mode. Within 3 milliseconds after the load current decreased, the supercapacitors could stop discharging entirely, and the battery and the output capacitor provided normal load power and then charged the supercapacitors. These results show that the power allocation strategy based on the hysteretic control principle has good dynamic-response ability.

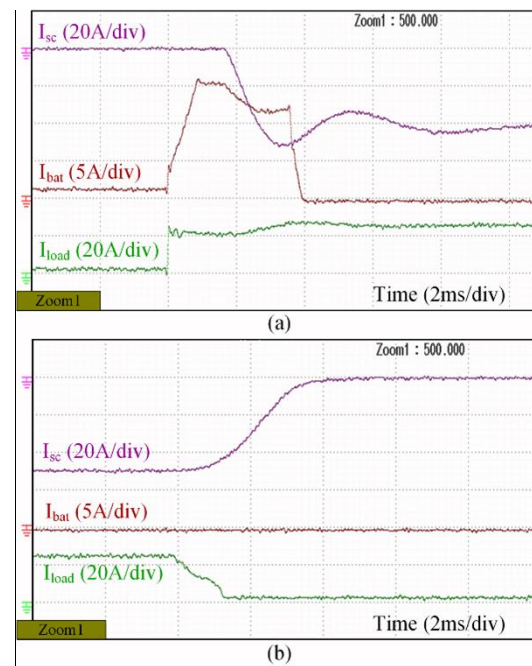


Figure 12. The dynamic experimental waveforms during converter operation mode switch: (a) buck mode to boost mode, (b) boost mode to buck mode.

Figure 13 shows the efficiency of the converter (buck mode) during the supercapacitor charging process. Since the charging current was fixed, the charging power depended on the supercapacitor pack voltage V_{SC} . In the voltage range from 40 V to 56 V, the converter maintained a charging efficiency above 95.84%. Figure 14 shows the efficiency of the converter (boost mode) at different levels of load power during the supercapacitor's discharging process. When the output power was constant at 2 kW, the efficiency during the entire discharge process was not less than 96.89%.

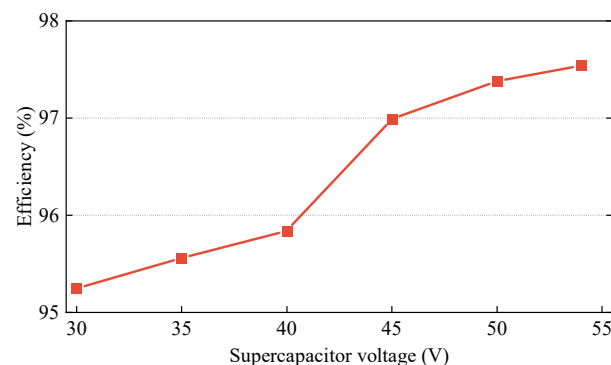


Figure 13. Efficiency of the converter (buck mode).

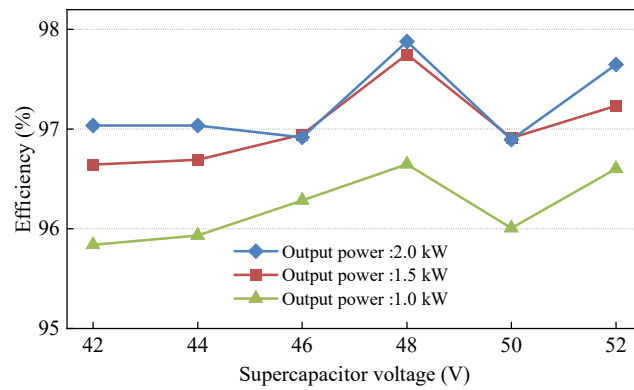


Figure 14. Efficiency of the converter (boost mode).

Figure 15 shows the total weight and energy utilization coefficient (EUC) of BESS and HESS under the same load, where the EUC is defined as the ratio of the total energy consumed by the load to the rated energy of the battery pack.

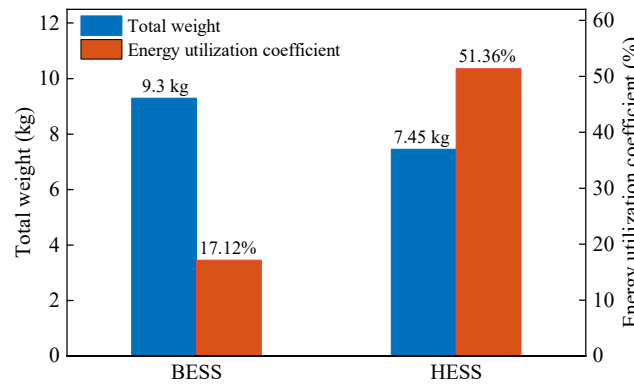


Figure 15. The total weight and energy utilization coefficient of BESS and HESS.

In BESS, the Li-ion battery pack with a rated capacity of 28.8 Ah was used to satisfy the peak load current, with a total weight of 9.3 kg, and the EUC was only 17.12%. In HESS, the battery pack with a rated capacity of 9.6 Ah was sufficient, so the EUC increased to 51.36%. The total weight of HESS was 7.45 kg, consisting of the Li-ion battery pack with a weight of 3.5 kg, the supercapacitor pack with a weight of 2.25 kg, and the DC–DC converter and control system with a total weight of 1.7 kg. The weight distribution of each device in HESS is shown in Figure 16.

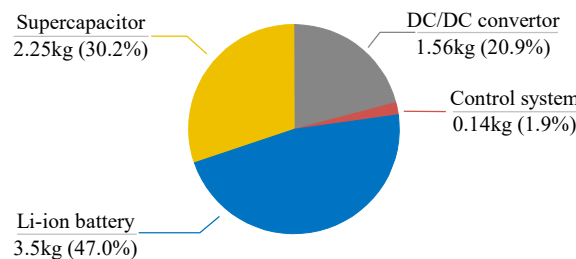


Figure 16. Weight distribution of each device in HESS.

Figure 17 shows the cost comparison between BESS and HESS. A 72V/28.8Ah Li-ion battery was used in BESS to meet the pulse power requirements of the load. In HESS, the capacity of a Li-ion battery was only 9.6 Ah, and the cost of a Li-ion battery was only 36.68% of BESS. Although the supercapacitor module and the bidirectional DC–DC converter were added to HESS, the total cost of HESS was only 59.07% of the cost of BESS due to the dramatic drop in the cost of Li-ion battery.

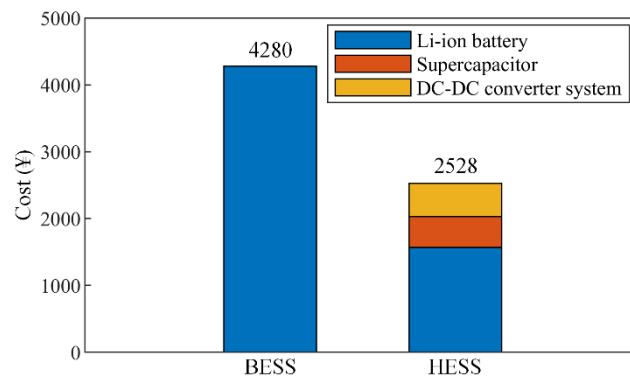


Figure 17. The cost comparison between BESS and HESS.

6. Conclusions

In this paper, a supercapacitor/battery semi-active HESS with a full current-type control strategy was proposed for pulsed power loads. The peak load power was allocated to the supercapacitors, and the normal load power was provided by the batteries. By directly controlling the output current of the DC–DC converter, the control system was simplified, and the model parameters were needless. The rated capacity of the battery pack was greatly reduced because the peak load power was allocated to the supercapacitors. The experimental results show that the full current-type control strategy has good control performance. Compared with the traditional BESS, the total weight of HESS was reduced by 19.89%, the energy utilization coefficient increased by 34.24%, and the cost was only 59.07% of the cost of BESS.

Author Contributions: Data curation, S.H.; Investigation, X.L.; Methodology, Z.D.; Project administration, W.L.; Writing—original draft, J.R.; Writing—review & editing, L.D. All authors have read and agreed to the published version of the manuscript.

Funding: This research received no external funding.

Conflicts of Interest: The authors declare no conflict of interest.

References

- Mamun, A.-A.; Liu, Z.; Rizzo, D.M.; Onori, S. An Integrated Design and Control Optimization Framework for Hybrid Military Vehicle Using Lithium-Ion Battery and Supercapacitor as Energy Storage Devices. *IEEE Trans. Transp. Electrification*. **2019**, *5*, 239–251. [\[CrossRef\]](#)
- Sertkaya, M.G.; Yilmaz, E.; Sanli, A.E.; Gunli, G. Comparison of power and energy density after full shunting-balancing in serial connected lithium-ion batteries and serial-connected supercapacitors. In Proceedings of the 2015 3rd International Renewable and Sustainable Energy Conference (IRSEC), Marrakech, Morocco, 10–13 December 2015; pp. 1–5.
- Mesbahi, T.; Khenfri, F.; Rizoug, N.; Bartholomeüs, P.; Moigne, P.L. Combined Optimal Sizing and Control of Li-Ion Battery/Supercapacitor Embedded Power Supply Using Hybrid Particle Swarm-Nelder-Mead Algorithm. *IEEE Trans. Sustain. Energy* **2017**, *8*, 59–73. [\[CrossRef\]](#)
- Gineste, V.; Gajewski, L.; Carron, C.; Rouzies, C.; Marec, A.; Sanchez, O. Li-ion battery/Supercapacitor Hybrid Power Supply (HPS) For Space Applications. In Proceedings of the 10th European Space Power Conference, Noordwijkerhout, The Netherlands, 13–17 April 2014; pp. 1–7.
- Dam, D.H.; Lee, H.H. Battery-inductor-supercapacitor hybrid energy storage system for DC microgrids. *J. Power Electron.* **2020**, *20*, 308–318. [\[CrossRef\]](#)
- Salah, I.B.; Bayoudhi, B.; Diallo, D. EV energy management strategy based on a single converter fed by a hybrid battery/supercapacitor power source. In Proceedings of the 2014 First International Conference on Green Energy ICGE, Sfax, Tunisia, 25–27 March 2014; pp. 246–250.
- Andreev, M.K. An Overview of Supercapacitors as New Power Sources in Hybrid Energy Storage Systems for Electric Vehicles. In Proceedings of the 2020 XI National Conference with International Participation (ELECTRONICA), Sofia, Bulgaria, 23–24 July 2020; pp. 1–4.
- Dezza, F.C.; Musolino, V.; Piegari, L.; Rizzo, R. Hybrid battery–supercapacitor system for full electric forklifts. *IET Electr. Syst. Transp.* **2018**, *9*, 16–23. [\[CrossRef\]](#)

9. Amjadi, Z.; Williamson, S.S. Power-Electronics-Based Solutions for Plug-in Hybrid Electric Vehicle Energy Storage and Management Systems. *IEEE Trans. Ind. Electron.* **2010**, *57*, 608–616. [[CrossRef](#)]
10. Song, Z.; Li, J.; Han, X.; Xu, L.; Lu, L.; Ouyang, M.; Hofmann, H. Multi-objective optimization of a semi-active battery/supercapacitor energy storage system for electric vehicles. *Appl. Energy* **2014**, *135*, 212–224. [[CrossRef](#)]
11. Kim, Y.; Raghunathan, V.; Raghunathan, A. Design and Management of Battery-Supercapacitor Hybrid Electrical Energy Storage Systems for Regulation Services. *IEEE Trans. Multi-Scale Comput. Syst.* **2017**, *3*, 12–24. [[CrossRef](#)]
12. Song, Z.; Hofmann, H.; Li, J.; Han, X.; Zhang, X.; Ouyang, M. A comparison study of different semi-active hybrid energy storage system topologies for electric vehicles. *J. Power Sources* **2015**, *274*, 400–411. [[CrossRef](#)]
13. Cao, J.; Emadi, A. A New Battery/UltraCapacitor Hybrid Energy Storage System for Electric, Hybrid, and Plug-In Hybrid Electric Vehicles. *IEEE Trans. Power Electron.* **2012**, *27*, 122–132.
14. Camara, M.B.; Gualous, H.; Gustin, F.; Berthon, A.; Dakyo, B. DC/DC Converter Design for Supercapacitor and Battery Power Management in Hybrid Vehicle Applications—Polynomial Control Strategy. *IEEE Trans. Ind. Electron.* **2010**, *57*, 587–597. [[CrossRef](#)]
15. Yuhimenko, Y.; Lerman, C.; Kuperman, A. DC Active Power Filter-Based Hybrid Energy Source for Pulsed Power Loads. *IEEE J. Emerg. Sel. Top. Power Electron.* **2015**, *3*, 1001–1010. [[CrossRef](#)]
16. Xiaoliang, H.; Curti, J.M.A.; Yoichi, H. Energy management strategy with optimized power interface for the battery supercapacitor hybrid system of Electric Vehicles. In Proceedings of the IECON 2013—39th Annual Conference of the IEEE Industrial Electronics Society, Vienna, Austria, 10–13 November 2013; pp. 4635–4640.
17. Song, Z.; Hofmann, H.; Li, J.; Hou, J.; Han, X.; Ouyang, M. Energy management strategies comparison for electric vehicles with hybrid energy storage system. *Appl. Energy* **2014**, *134*, 321–331. [[CrossRef](#)]
18. Hredzak, B.; Agelidis, V.G.; Jang, M. A Model Predictive Control System for a Hybrid Battery-Ultracapacitor Power Source. *IEEE Trans. Power Electron.* **2014**, *29*, 1469–1479. [[CrossRef](#)]
19. Ferreira, A.A.; Pomilio, J.A.; Spiazzi, G.; de Araujo Silva, L. Energy Management Fuzzy Logic Supervisory for Electric Vehicle Power Supplies System. *IEEE Trans. Power Electron.* **2008**, *23*, 107–115. [[CrossRef](#)]
20. Vinot, E.; Trigui, R. Optimal energy management of HEVs with hybrid storage system. *Energy Convers. Manag.* **2013**, *76*, 437–452. [[CrossRef](#)]
21. Hammani, A.; Sadoun, R.; Rizoug, N.; Bartholomeüs, P.; Barbedette, B.; Moigne, P.L. Influence of the management strategies on the sizing of hybrid supply composed with battery and supercapacitor. In Proceedings of the 2012 First International Conference on Renewable Energies and Vehicular Technology, Nabeul, Tunisia, 26–28 March 2012; pp. 1–7.
22. Sadoun, R.; Rizoug, N.; Bartholomeüs, P.; Barbedette, B.; Moigne, P.L. Optimal sizing of hybrid supply for electric vehicle using Li-ion battery and supercapacitor. In Proceedings of the 2011 IEEE Vehicle Power and Propulsion Conference, Chicago, IL, USA, 6–9 September 2011; pp. 1–8.
23. Sadoun, R.; Rizoug, N.; Bartholomeüs, P.; Moigne, P.L. Optimal architecture of the hybrid source (battery/supercapacitor) supplying an electric vehicle according to the required autonomy. In Proceedings of the 2013 15th European Conference on Power Electronics and Applications (EPE), Lille, France, 2–6 September 2013; pp. 1–7.
24. Yahaya, N.Z.; Begam, K.M.; Awan, M. Investigation of high frequency effects on soft-switched synchronous rectifier buck converter. In Proceedings of the 2009 IEEE Symposium on Industrial Electronics & Applications, Kuala Lumpur, Malaysia, 4–6 October 2009; pp. 525–529.
25. Do, X.-D.; Han, S.-K.; Lee, S.-G. Low power consumption for detecting current zero of synchronous DC-DC buck converter. In Proceedings of the 2012 International SoC Design Conference (ISOCC), Jeju Island, Korea, 4–7 November 2012; pp. 487–490.
26. Tseng, K.-C.; Chang, Y.-C.; Cheng, C.-A. Implementation and analysis of ultracapacitor charger in hybrid energy-storage system for electric-vehicle applications. *IET Power Electron.* **2020**, *13*, 1858–1864. [[CrossRef](#)]